A First Global View of Sub-Millimeter Radiances From the Arctic Weather Satellite

(article starts on next page)

AGU ADVANCING EARTH AND SPACE SCIENCES

Earth and Space Science

RESEARCH LETTER
10.1029/2025EA004893

A First Global View of Sub-Millimeter Radiances From the Arctic Weather Satellite

D. I. Duncan[1], **N. Bormann**[1], **M. D. Fielding**[1], **A. J. Geer**[1], **P. McEvoy**[2], **E. May**[2], and **P. Eriksson**[2]

[1]ECMWF, Reading, UK, [2]Chalmers University of Technology, Gothenburg, Sweden

Key Points:

- Arctic Weather Satellite is the first satellite providing real-time global measurements of sub-millimeter frequencies (300+ GHz)
- Its 325 GHz channels are more sensitive to ice clouds than the well-known 183 GHz humidity-sounding band
- Radiative transfer modeling can adequately simulate this frequency band for data assimilation and retrievals

Correspondence to:
D. I. Duncan,
david.duncan@ecmwf.int

Citation:
Duncan, D. I., Bormann, N., Fielding, M. D., Geer, A. J., McEvoy, P., May, E., & Eriksson, P. (2026). A first global view of sub-millimeter radiances from the Arctic Weather Satellite. *Earth and Space Science*, *13*, e2025EA004893. https://doi.org/10.1029/2025EA004893

Received 20 NOV 2025
Accepted 12 JUN 2026

Author Contributions:
Conceptualization: D. I. Duncan, A. J. Geer, P. Eriksson
Formal analysis: D. I. Duncan, M. D. Fielding, P. McEvoy, E. May
Funding acquisition: N. Bormann
Methodology: D. I. Duncan
Software: D. I. Duncan
Supervision: N. Bormann
Visualization: D. I. Duncan, M. D. Fielding
Writing – original draft: D. I. Duncan
Writing – review & editing: D. I. Duncan, N. Bormann, M. D. Fielding, A. J. Geer, P. McEvoy, E. May, P. Eriksson

Abstract The Arctic Weather Satellite (AWS) from the European Space Agency is a small satellite launched in August 2024 carrying a microwave radiometer for atmospheric sounding. AWS features the first satellite-borne sub-millimeter wavelength (> 300 GHz) channels for operational meteorology. This "sub-mm" band is more sensitive to scattering from ice clouds than traditional microwave frequencies and opens up new possibilities for measuring ice clouds and constraining their representations in atmospheric models. For example, 325 GHz radiances are roughly three times more sensitive to frozen water path than 183 GHz radiances. This letter explores how well sub-mm radiances are currently modeled by state-of-the-art radiative transfer simulators. It also highlights the novel information about ice clouds that can be exploited using these radiative transfer simulators, in the context of weather forecasting and physics-based retrievals.

Plain Language Summary A small, trail-blazing satellite was launched in 2024 that provides better sensitivity to ice cloud mass than ever before on a global scale. Using a new frequency band known as the sub-millimeter, the Arctic Weather Satellite provides unprecedented views of ice clouds in near-real time. Its new 325 GHz band is roughly three times more sensitive to ice clouds than the well-known 183 GHz band. This is a valuable additional resource for satellite meteorology and atmospheric models, and this short paper highlights some of the possibilities unlocked by these observations.

1. Introduction

Sensitivity to ice clouds varies considerably across the microwave spectrum (Geer et al., 2021). At microwave frequencies below 60 GHz, ice clouds barely attenuate microwave radiation. At these frequencies, rain and liquid clouds are more important due to differences in the refractive index of ice and water. Above 60 GHz, larger frozen particles such as snow and hail generate a scattering effect, but smaller ice particles impact the observations mainly above 200 GHz (Buehler et al., 2007; Evans et al., 1995). Newly launched satellite measurements at these higher frequencies allow us, for the first time, to explore the global radiative signature of smaller ice particles.

The promise of higher-frequency observations for better measurement of ice clouds has gained traction over recent years as the gaps in our knowledge of ice cloud distributions (Duncan & Eriksson, 2018; Eriksson et al., 2026; Waliser et al., 2009) remain a significant uncertainty in weather models (Geer et al., 2017) and climate change projections (Forster et al., 2021). One reason that higher frequencies are so sensitive to ice clouds is that particle size and wavelength become more similar, bringing their interaction with radiation into the Mie regime. For example, at 300 GHz, the wavelength is 1 mm, approaching the sizes of smaller cirrus cloud particles, which can be as small as 100 µm. In the Mie regime, particles generate scattering that is strongly dependent on details of their size, shape and orientation. These frequencies can thus infer not just the mass of ice clouds, but also microphysical information. At even higher frequencies that approach the infrared spectrum, ice clouds become strongly attenuating. This makes the region above 300 GHz, known as the sub-mm, uniquely placed to observe ice clouds.

Given the advantages of the sub-mm for ice cloud studies, there has been a push to observe these frequencies for use in operational meteorology. Field campaigns have measured sub-mm radiances from aircraft (Evans et al., 2005, 2012; Fox et al., 2017), permitting tests of radiative transfer models (RTMs) and particle scattering models (Pfreundschuh et al., 2022). Successful retrievals of cloud ice mass have been demonstrated using sub-mm limb sounder observations (Eriksson et al., 2014; Wu et al., 2008). EUMETSAT's next generation of polar-orbiters features the Ice Cloud Imager (ICI), with several sub-mm bands at 325, 448, and 664 GHz (Eriksson et al., 2020). ICI is expected to launch in 2026. Ahead of this, the trail-blazing small satellite AWS was

Table 1
Selected Arctic Weather Satellite Channels

Ch. #	Frequency (GHz)	Bandwidth (MHz)
9	89.0	4,000
10	165.5	2,800
11	176.311	2,000
12	178.811	2,000
13	180.311	1,000
14	181.511	1,000
15	182.311	500
16	325.15 ± 1.2	2 × 800
17	325.15 ± 2.4	2 × 1,200
18	325.15 ± 4.1	2 × 1,800
19	325.15 ± 6.6	2 × 2,800

Note. Here we focus on the higher frequencies, but AWS also has a suite of channels from 50 to 57 GHz not shown here.

launched by European Space Agency (ESA) in summer 2024. AWS features four channels in the 325 GHz water vapor absorption band and is the first satellite to provide sub-mm radiances for operational applications.

This letter showcases some of the newfound sensitivity to frozen hydrometeors unlocked by these first 325 GHz channels. Accurate simulation of this new spectral region is key to its exploitation in data assimilation and physical retrievals, and this is examined with comparison to state-of-the-art RTMs.

2. The Arctic Weather Satellite

The AWS is a small satellite with a microwave radiometer as its sole payload (Eriksson et al., 2025). Developed following a "new space" approach and acting as a pathfinder for the EPS-Sterna constellation from EUMETSAT, AWS was built and tested on an accelerated timeline and launched in August 2024. As well as the new channels at 325 GHz, the AWS radiometer measures bands near 50 and 183 GHz known to be impactful when assimilated in numerical weather prediction (NWP) systems (Duncan et al., 2021), and its polar orbit provides observations globally with frequent sampling over the Arctic.

The radiometer on AWS is a cross-track microwave sounder with 19 total channels (Table 1; see Eriksson et al. (2025) for further instrument details). Its four sub-mm channels measure on both sides of the 325 GHz water vapor absorption line, providing similar humidity profiling capabilities as the 183 GHz channel suite in clear skies, as first envisioned by Gasiewski (1992). But due to the higher frequencies measured, these channels exhibit greater sensitivity to ice particles and can provide a better view of ice cloud mass than any previously available in the global observing system.

2.1. Degrees of Freedom

To quantify the information added by the sub-mm band on AWS, we analyze the measurements' degrees of freedom (DoF) (Rodgers, 2000). DoF is here calculated following Eriksson et al. (2020) and can be interpreted as the number of orthogonal pieces of information contained in the measurements. This is a statistical measure that does not link directly to specific geophysical variables. The analysis is applied to ARTS simulated measurements (described in Section 4) and binned by frozen water path (FWP).

Figure 1a shows DoF with and without the sub-mm channels. Using only observations between 165 and 182 GHz, DoF remains constant at 4 across the full FWP range, in contrast to the 6 channels available. Likely the information associated with these DoF varies across the FWP range. For low FWP the information is on the water vapor profile and possibly also the surface, in dry conditions. At high FWP, the information is likely dominated by

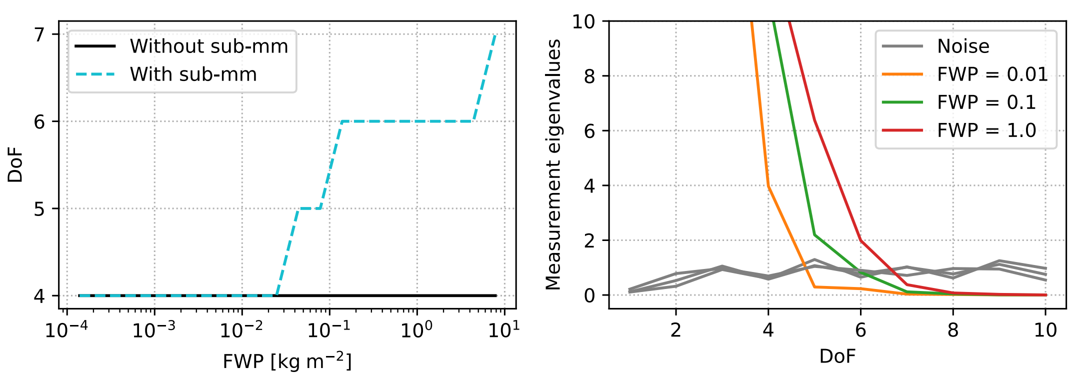

Figure 1. Degrees of freedom (DoF) analysis of Arctic Weather Satellite measurements. Panel (a) shows the DoF as a function of frozen water path (FWP), with and without the sub-mm channels. Panel (b) shows the eigenvalues, used to calculate the DoF, per FWP bin. Also shown in panel (b) is the instrument noise projected onto the eigenvector space of the measurements.

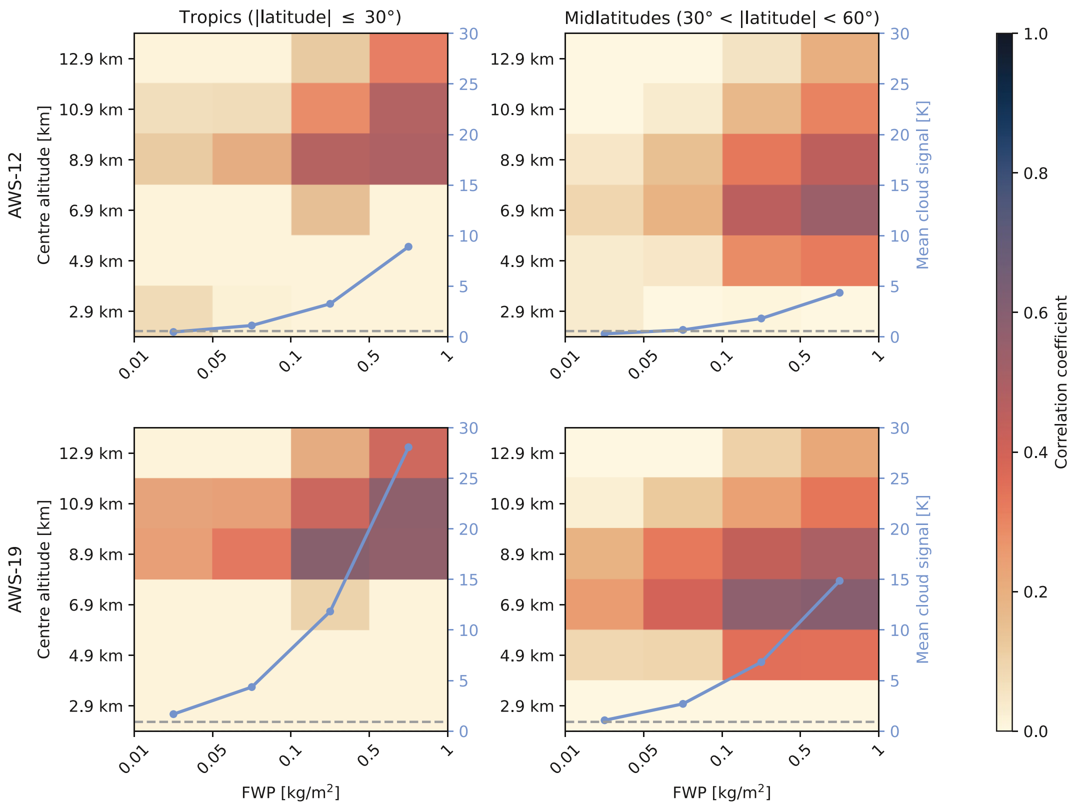

Figure 2. Correlations between frozen water path (FWP) (mean inside 2 km layers) and cloud signal (clear-sky minus all-sky TB). Each correlation value is calculated for all cases with an FWP inside the range indicated on the *x*-axis. The blue line shows the mean cloud signal for cases within the FWP bin. Estimated levels of instrument noise were added to the simulated cloud signals, and the standard deviation of this noise is indicated by the gray dashed line. The data used are ARTS simulations (see Section 4).

ice cloud and precipitation. Including the sub-mm channels leads to an increase of DoF with FWP: the DoF rises to 5 slightly above FWP = 10 g m^{-2} and reaches a maximum of 7 at the highest FWP. We believe this shows the sub-mm channels increase information on the vertical profile of ice mass, though it may also reflect increased information on mean particle size (May & Eriksson, 2025). The DoF measure alone cannot distinguish.

Figure 1b illustrates how the DoF calculation of Eriksson et al. (2020) is a count of the number of eigenvalues that are above the instrument noise. This count is naturally quantized, different from the continuous number provided by the standard approach (Rodgers, 2000), but it is arguably simpler and clearer to compute. The results shown in this panel are based on the full channel set of AWS with the sub-mm channels included. As the FWP increases, more eigenvalues are above the noise.

2.2. Signal for Frozen Water Path

Another way to probe the novelty of the 325 GHz band is to interrogate the signal it provides for detecting atmospheric ice. Compared to the 183 GHz band (AWS-12 at 178.8 GHz), brightness temperature (TB) depressions from scattering in the 325 GHz band (AWS-19 at 325 ± 6.6 GHz) are significant at lower FWP values. This is shown in Figure 2 in two ways, using the same data set as the DoF analysis. First, cloud signals (defined here as clear-sky minus all-sky TB) are shown as a function of FWP for AWS channels 12 and 19, split into tropical and midlatitude locations. Second, Spearman correlation coefficients were computed between 2 km layers of FWP and the top of atmosphere TB, shown in the shaded boxes. This is a way to view both the TB sensitivity and the vertical information, whilst including realistic instrument noise and covering a wide range of atmospheric conditions.

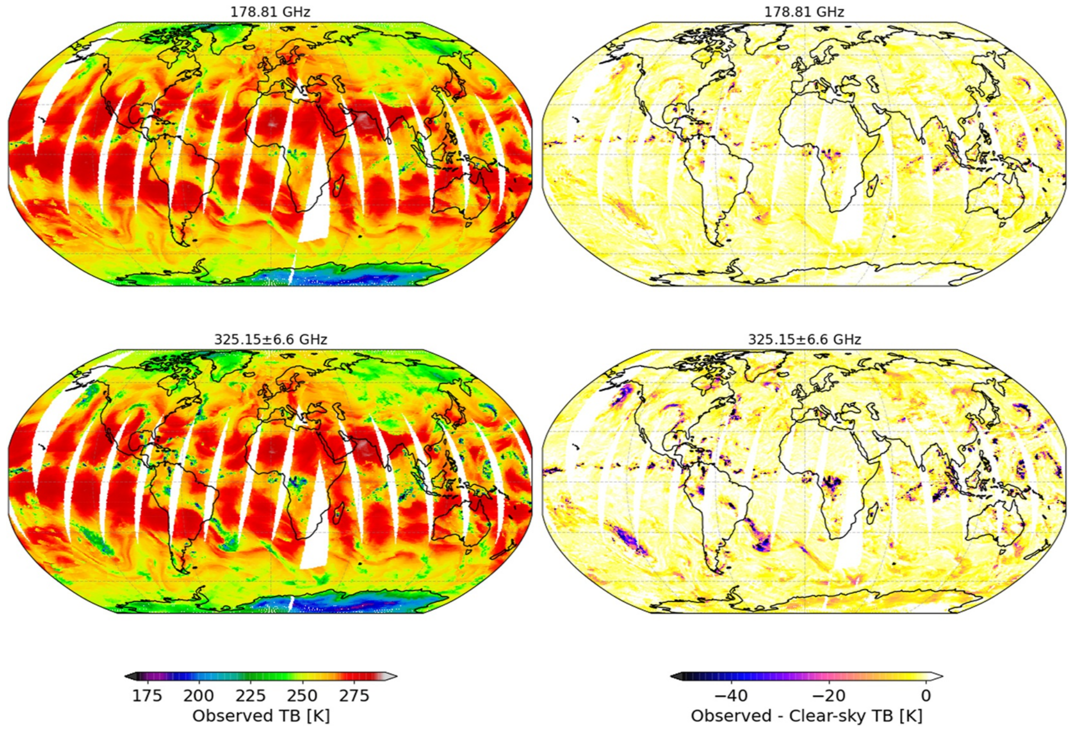

Figure 3. Arctic Weather Satellite data from 9 November 2024, 9–21 UTC. The left column shows observed TBs at channels 12 (178.8 GHz) and 19 (325 ± 6.6 GHz); the right column shows cloud signals, given by observed TB minus the simulated clear-sky TB from the ECMWF short-range forecast.

Seen in Figure 2, AWS-19 shows higher correlations than AWS-12 for the FWP range considered. This result is especially noteworthy as AWS-19 is noisier than AWS-12 (0.80 vs. 0.39 K from Eriksson et al. (2025)), and higher instrument noise will decrease correlations. The 325 GHz channels produce about 2–6 times the TB impact for the same FWP, permitting detection of cloud ice for thinner clouds than before. To put this in perspective for retrievals and data assimilation, where 3 K observation error might be used for such channels, a 0.1kg m^{-2} cloud signal is generally within the noise at 183 GHz but clearly visible at 325 GHz.

3. Results

3.1. Global View

A global picture of AWS observations is found in Figure 3, showing observed TBs from two AWS channels with similar clear-sky Jacobians for humidity, 178.8 and 325 ± 6.6 GHz (see Figure 12 in Eriksson et al. (2025)). Data are taken from a 12-hr period on 9 November 2024. The patterns and magnitudes are quite similar, but closer examination reveals colder measurements at 325 ± 6.6 GHz in cloudy regions. To tease out this difference, the right column shows the impact of clouds on the measured TBs, calculated as a difference between observations and simulations without clouds and precipitation; the simulated fields come from the ECMWF short-range forecast, simulated using RTTOV-SCATT v13.2 (Geer et al., 2021). From the cloud impacts on the right, it is clear that scattering signals greater than a few degrees are spatially limited in the 178.8 GHz channel but much more common at 325 ± 6.6 GHz. There are also much more frequent large cloud signals in the sub-mm band, particularly in the storm track regions.

From this global view, we can zoom in to examine the dynamic range of 325 GHz radiances in extreme conditions. Figure 4 left panels show observations of a tropical cyclone just south of Hong Kong (and east of Hainan Island) that is hardly visible at the global scale. The figure shows channels from three of the bands measured by AWS: 89, 178.8, and 325 ± 6.6 GHz. The 89 and 178.8 GHz bands are well observed from numerous polar-orbiting satellites but it is clear from this image that the sub-mm radiances highlight atmospheric features that are absent or more muted at lower frequencies.

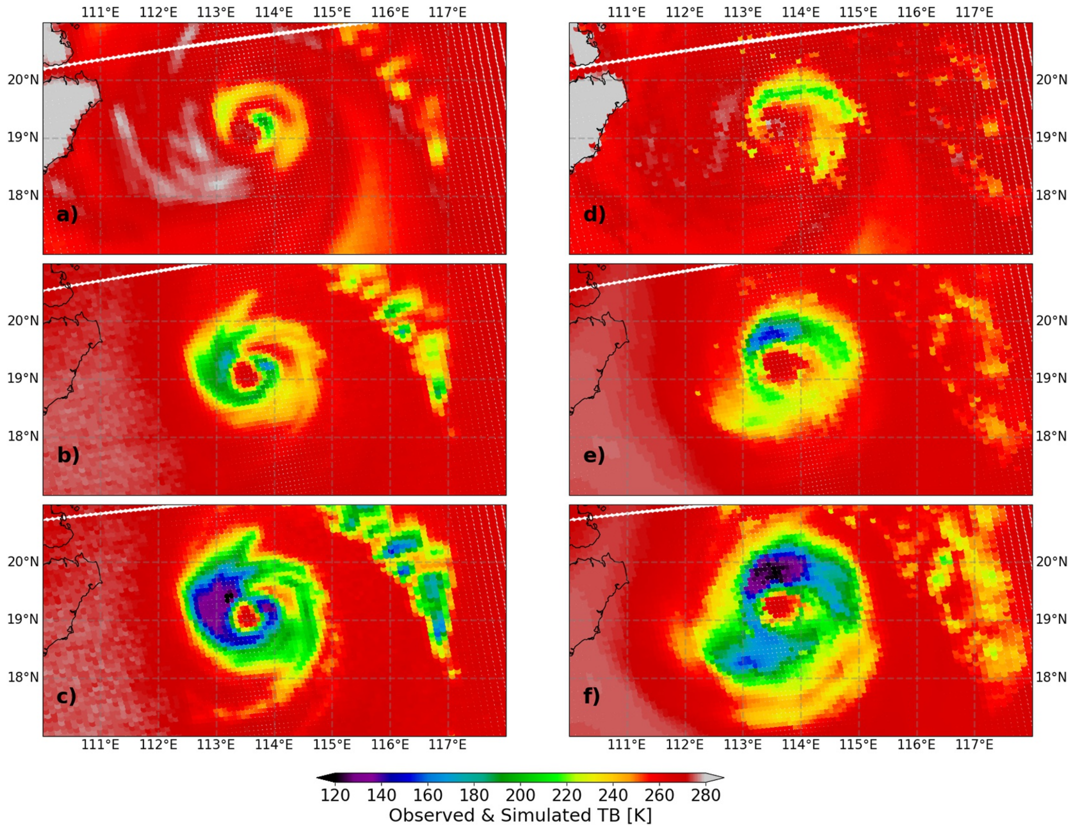

Figure 4. Arctic Weather Satellite observations in the left column at (a) 89.0, (b) 178.8, and (c) 325 ± 6.6 GHz over Typhoon Yinxing, 9 November 2024. The right column (d–f) shows model equivalents from the ECMWF short-range forecast in observation space for the same frequencies.

This tropical cyclone, named Yinxing, had re-intensified to category 3 on 9 November after earlier affecting the Phillipines. In the AWS observations, this small but intense cyclone exhibits a drop in TBs of approximately 150 K between eye and eyewall at 325 ± 6.6 GHz—a remarkable radiometric contrast across a distance of just 50 km. In the outer rain band northeast of the cyclone, the extent of the cirrus shield around convective cores is also much clearer in the sub-mm image; much of this cirrus cover is apparently invisible at lower frequencies.

The right column of Figure 4 shows the ECMWF short-range forecast of this cyclone in observation space, that is, the model background, simulated by RTTOV-SCATT. The forecasted eye is roughly correct, with a very strong circulation and very cold TBs at 178.8 and 325 ± 6.6 GHz. Although the most intense convection is misplaced (possibly due to stochastic errors or limitations of the forecast model), the magnitude of TB depressions appears fairly realistic from RTTOV-SCATT, a topic we will return to in the following section.

3.2. Antarctic Snowstorm

Another ESA mission, Earth Clouds, Aerosol and Radiation Explorer (EarthCARE), was launched just a few months before AWS (Wehr et al., 2023). Its payload includes the first ever space-borne Doppler cloud radar (Cloud Profiling Radar), providing unprecedented capabilities for studying cloud vertical structures. We can thus use space-time matchups of AWS and EarthCARE to examine the signals that AWS sub-mm channels provide. AWS and EarthCARE cross paths only near the poles due to their specific sun-synchronous orbits, producing many opportunities for the study of snowfall and polar clouds. Figure 5 shows a matched overpass of EarthCARE and AWS over Antarctica, capturing a heavy snowstorm only 15 min apart.

The Antarctic snowstorm peaks in intensity near the coast, as seen in the radar reflectivity profile of Figure 5a. The Doppler velocities in Figure 5b show the widespread precipitation in this transect, plus an interesting gravity wave feature of alternating up- and down-drafts north of the heaviest snowfall. Matched AWS TBs in Figure 5c

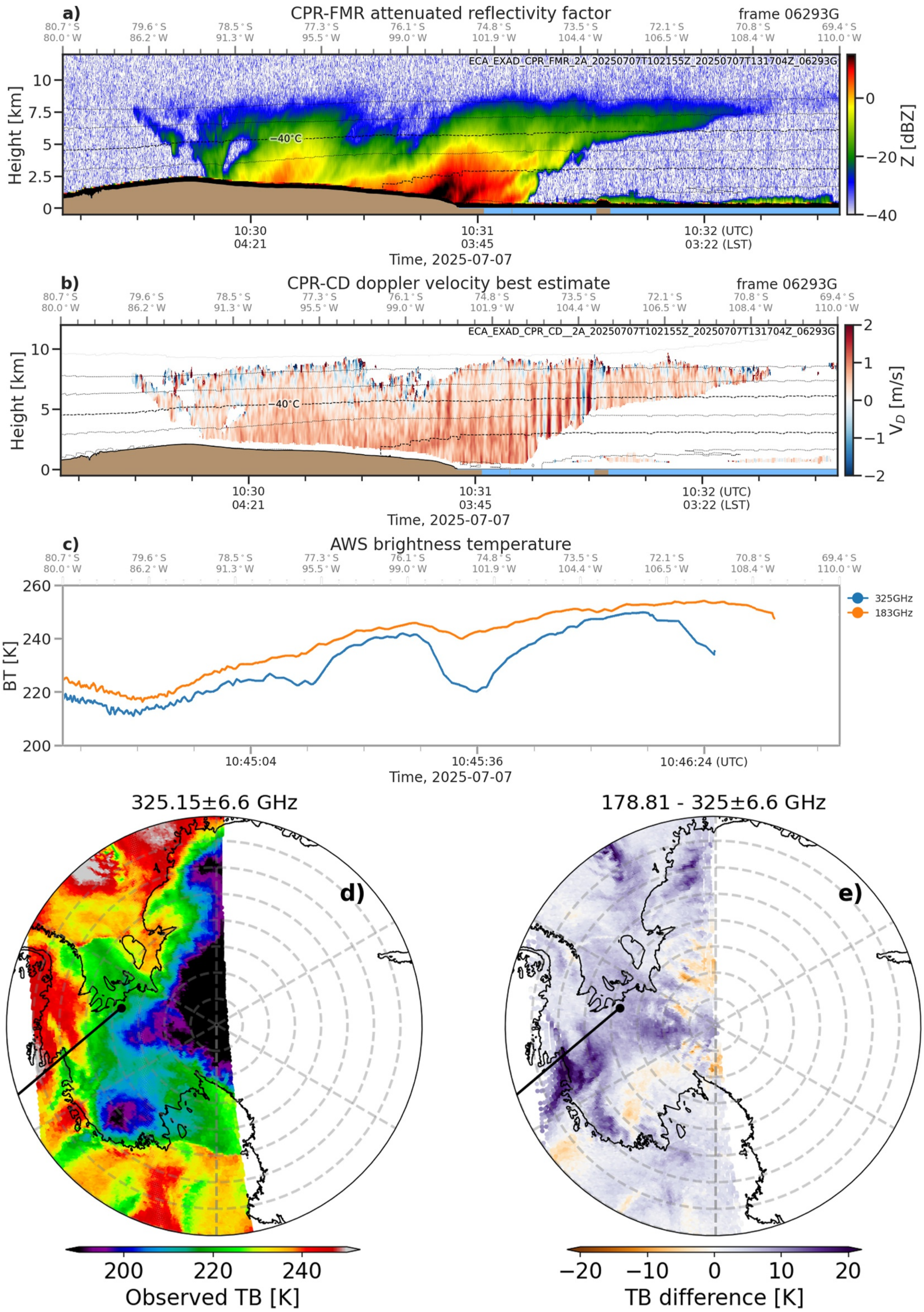

Figure 5. EarthCARE and Arctic Weather Satellite (AWS) matched observations for a snowfall event over Antarctica on 7 July 2025. Panels show (a) Cloud Profiling Radar (CPR) reflectivity, (b) CPR Doppler velocity, and (c) matched AWS observations from 178.8 and 325 ± 6.6 GHz. In panels (d, e), the swath of these AWS channels is shown with the EarthCARE segment displayed in black, with (d) 325 ± 6.6 GHz and the difference of (e) 325 ± 6.6 and 178.8 GHz.

10.1029/2025EA004893

show two noticeable dips in 325 ± 6.6 GHz, coincident with the two regions of maximal reflectivities near 78°S and 75°S.

This change in TB is much stronger at 325 ± 6.6 GHz than in the 178.8 GHz channel—roughly a 20 K depression at its height—showcasing the greater sensitivity to snowfall in the sub-mm band. In contrast, the 178.8 GHz channel exhibits little variation in TB over this precipitating scene. Observed sub-mm TBs from AWS are seen in Figure 5d, displaying a notably smaller dynamic range here when compared to tropical deep convection in the previous figure. The difference of the bands is seen in Figure 5e, with the blue colors indicating greater scattering at 325 ± 6.6 GHz. This case exemplifies the finding of Figure 1, with the new sub-mm channels adding information in scenes with significant frozen water aloft, verified here by the EarthCARE radar.

4. Fidelity of Ice Cloud Simulations in the Sub-mm

So far we have examined measured radiances, but to convert these into actionable geophysical information (via data assimilation or retrieval schemes) requires accurate radiative transfer modeling. In preparation for sub-mm observations from ICI, numerous aspects of RTMs have been improved in recent years. For example, RTMs previously simulated frequencies up to 200 or 300 GHz, and required expanded surface emissivity models (Kilic et al., 2023), improved spectroscopy (Mattioli et al., 2019; Turner et al., 2022), and updated particle scattering models (Ekelund et al., 2018). The AWS observations provide the first chance to validate some of these developments globally.

Beyond fundamental radiative transfer developments, it has been equally important to improve ice and snow microphysics within RTMs. Cloud microphysics are not well represented by forecast models and are assumed a priori and/or inferred from observations. For example, Geer (2021) used parameter estimation to fit radiative transfer simulations to existing satellite observations covering 19–190 GHz. In particular, thinner cloud ice should be mostly invisible near 183 GHz (as illustrated in Figure 4) and to achieve this, it must be represented by relatively small and less dense particles. The new 325 GHz observations give an opportunity to test the extrapolation of these tuned assumptions into the sub-mm, particularly this microphysical description of the ice clouds.

Here AWS observations are compared with simulations from two state-of-the-art RTMs. RTTOV-SCATT (Bauer et al., 2006) is a fast RTM that is used operationally by various NWP centers to simulate hundreds of millions of observations daily. ARTS (Buehler et al., 2025) is a vector RTM often used as a reference model for detailed absorption and scattering calculations (Barlakas & Eriksson, 2020; Brogniez et al., 2016).

RTTOV-SCATT is applied to the ECMWF operational short-range forecast (i.e., model background), which uses the Integrated Forecasting System (IFS) Cycle 49r1 (ECMWF, 2024) run at 9 km horizontal resolution. These simulations use RTTOV-SCATT version 13.2 with particle scattering properties described by Geer et al. (2021). Here the observations are averaged into 20 km super-observations (superobs) to facilitate exact matches between the 183 and 325 GHz feedhorns. The AWS fields of view are approximately 10 km at nadir, so this also better aligns with the 30–40 km effective model resolution of the IFS for clouds and precipitation (Duncan et al., 2024).

The ARTS simulations correspond to CloudSat overpasses in 2015, using ice water content fields derived from CloudSat radar reflectivities and supplemented with ERA5 atmospheric and surface data (Hersbach et al., 2020). Each simulation employs one of five randomly selected particle models, characterized by an ice crystal habit and particle size distribution. The particle models, and the full simulation framework, follow the approach of May et al. (2024), adapted for AWS. Habits are taken from the ARTS single scattering database (Ekelund et al., 2018) with DISORT used as the scattering solver (Buras et al., 2011). The ARTS observations are also averaged over 20 km.

An important validation of RTMs is whether they can reproduce the distribution and dynamic range of observed radiances. Figure 6a provides probability density functions (PDFs) of the same matched pair of 183 and 325 GHz observations already examined, spanning all data over ice-free oceans from a 10-day period in July 2025. The RTTOV simulations match these observations exactly in space and time, but note the ARTS simulations are from CloudSat tracks covering all of 2015. Although not concurrent with July 2025, this period should provide sufficient samples to enable RTM performance comparison. The PDFs for IFS and ARTS closely match observations at the warm end, but significant deviations between IFS and observations emerge for cloudy scenes, with too many lightly scattering scenes and not enough of the coldest scenes in the IFS short-range forecasts. As expected,

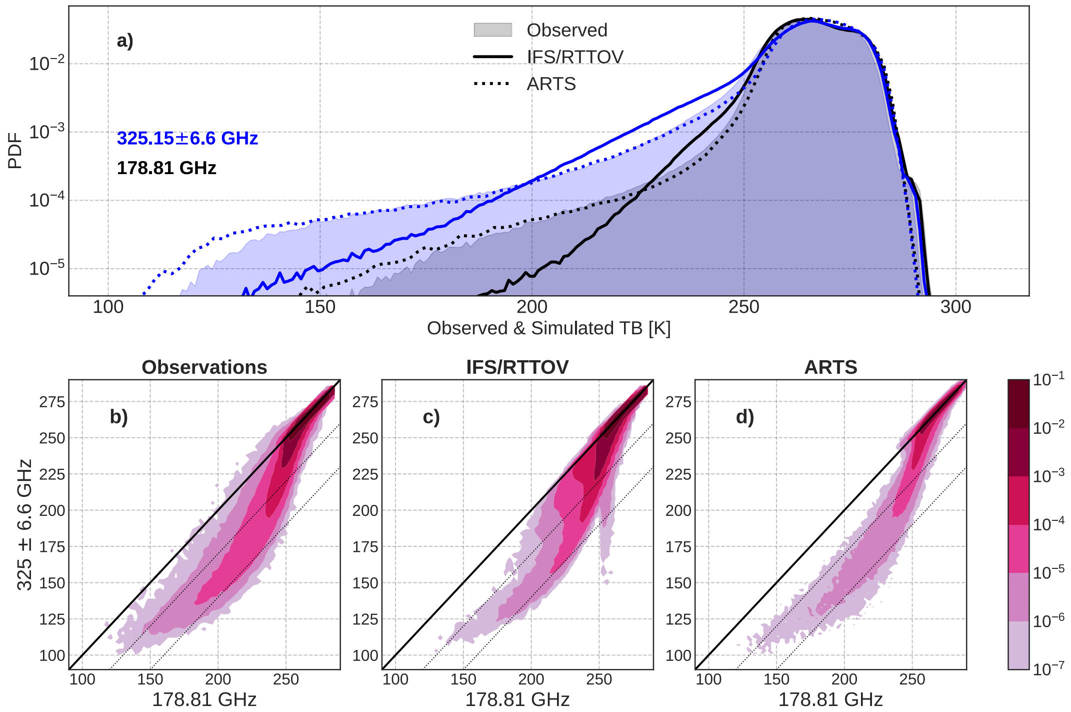

Figure 6. Probability density functions (PDFs) of observed and simulated TBs from 178.8 to 325 ±6.6 GHz. Panel (a) shows observed PDFs (shaded) alongside simulated values from Integrated Forecasting System (IFS) short-range forecasts (solid) and ARTS (dotted). Panels (b–d) show 2D PDFs of scattering signals between the same channels for (b) observations, (c) IFS, and (d) ARTS; dashed lines denote 30 and 60 K differences. See text for details on the data.

the tail of the observed PDF for the sub-mm channel is much longer than its 183 GHz counterpart, with TBs below 150 K relatively common. The peaks of the observed PDFs are closely matched, reflecting the channels' similar humidity sensitivity in clear skies.

Validation of the simulations is a test for both the RTM and the underlying forecast model. For example, even if the RTM can simulate the clouds perfectly, the PDFs will be mismatched if the forecast model has too few clouds overall. It is clear that in both frequency bands, the IFS simulations have too few heavily scattering scenes and too many lightly scattering scenes. This is a long-standing issue in comparisons between observations and simulations from IFS and RTTOV, with many possible explanations (Geer, 2021). The ARTS simulations do a better job of matching the observed PDF, albeit slightly underestimating the frequency of lightly scattering scenes with slightly too many very cold scenes.

Some of the differences between RTTOV-SCATT and ARTS may be explained by the different choices of ice particle models, as well as different sources of ice cloud profile, respectively from the IFS model and CloudSat retrievals. But when evaluated using the same theoretical ice cloud profiles, RTTOV-SCATT is known to produce less intense TB depressions compared to ARTS (Barlakas et al., 2022). This is attributed to the use of a fast but simplified delta-Eddington scattering solver in RTTOV-SCATT, compared to the more sophisticated multiple ordinate solver used in ARTS. In any case, for both RTMs, the key message here lies in the relative performance—the 325 GHz simulations' accuracy is on par with that achieved in the well-known 183 GHz band.

Lastly, we examine the relative scattering signals between the matched 183 and 325 GHz channels to see how the relative differences of the simulations compare with the observations. Figures 6b–6d hold 2D PDFs of the channel pair analyzed above. Although the time periods differ, the same banana shape appears in which TB depressions for heavily scattering scenes are frequently 30–60 K deeper in the 325 GHz band than at 183 GHz. At the very cold TBs of deep convective cloud scenes, the observations show similar scattering magnitudes in the two frequency bands, with some observations near the 1-to-1 line. This phenomenon is not reflected well in the simulations and may indicate suboptimal particle assumptions in deep convective cores. The ARTS model performs better in this respect than IFS/RTTOV, but neither captures the rare cases in which both TBs are approximately 125 K, for instance.

5. Conclusions

The higher frequencies observed by AWS open up new possibilities of measuring ice clouds and snow. When compared to the well-known 183 GHz band, sensitivity to thinner ice clouds is enhanced and larger scattering signals are observed in scenes from polar snowstorms to typhoons. Despite representing a fresh spectral region, existing RTMs perform very well at 325 GHz thanks to the detailed preparations for sub-mm radiative transfer that have been made by the community in recent years. For example, RTTOV-SCATT already simulates 325 GHz measurements with sufficient fidelity for operational assimilation in global NWP (Duncan et al., 2026), though improvements should be pursued in modeling of deep convective cores and ensuring microphysical consistency across the spectrum, just to name two future avenues for research. Over the coming years, and with a wider range of sub-mm observations from ICI, the hope is that uncertainties in the magnitude and distribution of atmospheric ice mass will improve as this new band is more fully utilized.

Conflict of Interest

The authors declare no conflicts of interest relevant to this study.

Availability Statement

AWS level 1 radiances are available via the EUMETSAT Data Store (https://data.eumetsat.int/data/map/EO:EUM:DAT:0905, registration required). EarthCARE radar data are available from JAXA (https://eolp.jaxa.jp/EarthCARE_CPR_L1B_CPR_NOM.html, registration required). ARTS is available from https://radiativetransfer.org, with the code visible on github (https://github.com/atmtools/arts/tree/v2.6.x) for the version used here, v2.6. RTTOV-SCATT v13.2 is available from the NWP-SAF (https://nwp-saf.eumetsat.int/). It is not currently possible to permanently archive or curate the large volume of data produced by experimental runs of an NWP system. However, a version of the ECMWF model is available for researchers (https://confluence.ecmwf.int/display/OIFS/About+OpenIFS) with full documentation of the data assimilation system also available for IFS Cycle 49r1, the version used here (https://www.ecmwf.int/en/publications/ifs-documentation).

Acknowledgments

Thank you to the three anonymous reviewers for their constructive feedback. Thanks to EUMETSAT for the support to examine early AWS data (Contract RFQ/21/1383948), especially Sabatino Di Michele, Christophe Accadia, and Paolo Colucci. Thanks to Shannon Mason (ECMWF) for help with EarthCARE data visualization. Also thanks to Tony McNally (ECMWF) for reviewing the manuscript. Thanks as well to the Swedish National Space Agency (2021-00077) for supporting this work at Chalmers University.

References

Barlakas, V., & Eriksson, P. (2020). Three dimensional radiative effects in passive millimeter/sub-millimeter all-sky observations. *Remote Sensing*, *12*(3), 531. https://doi.org/10.3390/rs12030531

Barlakas, V., Galligani, V. S., Geer, A. J., & Eriksson, P. (2022). On the accuracy of RTTOV-SCATT for radiative transfer at all-sky microwave and submillimeter frequencies. *Journal of Quantitative Spectroscopy and Radiative Transfer*, *283*, 108137. https://doi.org/10.1016/j.jqsrt.2022.108137

Bauer, P., Moreau, E., Chevallier, F., & O'Keeffe, U. (2006). Multiple-scattering microwave radiative transfer for data assimilation applications. *Quarterly Journal of the Royal Meteorological Society*, *132*(617), 1259–1281. https://doi.org/10.1256/qj.05.153

Brogniez, H., English, S., Mahfouf, J. F., Behrendt, A., Berg, W., Boukabara, S., et al. (2016). A review of sources of systematic errors and uncertainties in observations and simulations at 183 GHz. *Atmospheric Measurement Techniques*, *9*(5), 2207–2221. https://doi.org/10.5194/amt-9-2207-2016

Buehler, S. A., Jiménez, C., Evans, K. F., Eriksson, P., Rydberg, B., Heymsfield, A. J., et al. (2007). A concept for a satellite mission to measure cloud ice water path, ice particle size, and cloud altitude. *Quarterly Journal of the Royal Meteorological Society*, *133*(S2), 109–128. https://doi.org/10.1002/qj.143

Buehler, S. A., Larsson, R., Lemke, O., Pfreundschuh, S., Brath, M., Adams, I., et al. (2025). The atmospheric radiative transfer simulator ARTS, version 2.6 — Deep python integration. *Journal of Quantitative Spectroscopy and Radiative Transfer*, *341*, 109443. https://doi.org/10.1016/j.jqsrt.2025.109443

Buras, R., Dowling, T., & Emde, C. (2011). New secondary-scattering correction in DISORT with increased efficiency for forward scattering. *Journal of Quantitative Spectroscopy and Radiative Transfer*, *112*(12), 2028–2034. https://doi.org/10.1016/j.jqsrt.2011.03.019

Duncan, D. I., Bormann, N., Crepulja, M., Dahoui, M., Geer, A. J., Accadia, C., et al. (2026). Arctic weather satellite assessment and assimilation at ECMWF. *EGUsphere*, *2026*, 1–29. https://doi.org/10.5194/egusphere-2026-712

Duncan, D. I., Bormann, N., Geer, A. J., & Weston, P. (2024). Superobbing and thinning scales for all-sky humidity sounder assimilation. *Monthly Weather Review*, *152*(8), 1821–1837. https://doi.org/10.1175/MWR-D-24-0020.1

Duncan, D. I., Bormann, N., & Hólm, E. (2021). On the addition of microwave sounders and numerical weather prediction skill. *Quarterly Journal of the Royal Meteorological Society*, *147*(740), 3703–3718. https://doi.org/10.1002/qj.4149

Duncan, D. I., & Eriksson, P. (2018). An update on global atmospheric ice estimates from satellite observations and reanalyses. *Atmospheric Chemistry and Physics*, *18*(15), 11205–11219. https://doi.org/10.5194/acp-18-11205-2018

ECMWF. (2024). IFS documentation CY49R1 - Part II: Data assimilation. In *(chap. 2). Author*. https://doi.org/10.21957/105cb1333c

Ekelund, R., Brath, M., Mendrok, J., & Eriksson, P. (2018). ARTS microwave single scattering properties database (version 1.0.0) (Tech. Rep.). https://doi.org/10.5281/zenodo.1175573

Eriksson, P., Baró Pérez, A., Müller, N., Hallborn, H., May, E., Brath, M., et al. (2026). Advancements and continued challenges in observations and global modelling of atmospheric ice mass. *Atmospheric Chemistry and Physics*, *26*(4), 2741–2768. https://doi.org/10.5194/acp-26-2741-2026

Eriksson, P., Emrich, A., Kempe, K., Riesbeck, J., Aljarosha, A., Auriacombe, O., et al. (2025). The Arctic weather satellite radiometer. *Atmospheric Measurement Techniques*, *18*(18), 4709–4729. https://doi.org/10.5194/amt-18-4709-2025

Eriksson, P., Rydberg, B., Mattioli, V., Thoss, A., Accadia, C., Klein, U., & Buehler, S. A. (2020). Towards an operational ice cloud imager (ICI) retrieval product. *Atmospheric Measurement Techniques*, *13*(1), 53–71. https://doi.org/10.5194/amt-13-53-2020

Eriksson, P., Rydberg, B., Sagawa, H., Johnston, M. S., & Kasai, Y. (2014). Overview and sample applications of SMILES and Odin-SMR retrievals of upper tropospheric humidity and cloud ice mass. *Atmospheric Chemistry and Physics*, *14*(23), 12613–12629. https://doi.org/10.5194/acp-14-12613-2014

Evans, K. F., Turk, J., Wong, T., & Stephens, G. L. (1995). A bayesian approach to microwave precipitation profile retrieval. *Journal of Applied Meteorology*, *34*(1), 260–279. https://doi.org/10.1175/1520-0450-34.1.260

Evans, K. F., Wang, J. R., Racette, P. E., Heymsfield, G., & Li, L. (2005). Ice cloud retrievals and analysis with the compact scanning submillimeter imaging radiometer and the cloud radar system during CRYSTAL FACE. *Journal of Applied Meteorology*, *44*(6), 839–859. https://doi.org/10.1175/JAM2250.1

Evans, K. F., Wang, J. R., Starr, O., Heymsfield, G., Li, L., Tian, L., et al. (2012). Ice hydrometeor profile retrieval algorithm for high-frequency microwave radiometers: Application to the CoSSIR instrument during TC4. *Atmospheric Measurement Techniques*, *5*(9), 2277–2306. https://doi.org/10.5194/amt-5-2277-2012

Forster, P., Storelvmo, T., Armour, K., Collins, W., Dufresne, J.-L., Frame, D., et al. (2021). The Earth's energy budget, climate feedbacks, and climate sensitivity. In V. Masson-Delmotte, P. Zhai, A. Pirani, S. L. Connors, C. Péan, S. Berger, et al. (Eds.), *Climate change 2021: The physical science basis. Contribution of working group i to the sixth assessment report of the intergovernmental panel on climate change* (pp. 923–1054). Cambridge University Press. https://doi.org/10.1017/9781009157896.009

Fox, S., Lee, C., Moyna, B., Philipp, M., Rule, I., Rogers, S., et al. (2017). ISMAR: An airborne submillimetre radiometer. *Atmospheric Measurement Techniques*, *10*(2), 477–490. https://doi.org/10.5194/amt-10-477-2017

Gasiewski, A. (1992). Numerical sensitivity analysis of passive EHF and SMMW channels to tropospheric water vapor, clouds, and precipitation. *IEEE Transactions on Geoscience and Remote Sensing*, *30*(5), 859–870. https://doi.org/10.1109/36.175320

Geer, A. J. (2021). Physical characteristics of frozen hydrometeors inferred with parameter estimation. *Atmospheric Measurement Techniques*, *14*(8), 5369–5395. https://doi.org/10.5194/amt-14-5369-2021

Geer, A. J., Baordo, F., Bormann, N., Chambon, P., English, S. J., Kazumori, M., et al. (2017). The growing impact of satellite observations sensitive to humidity, cloud and precipitation. *Quarterly Journal of the Royal Meteorological Society*, *143*(709), 3189–3206. https://doi.org/10.1002/qj.3172

Geer, A. J., Bauer, P., Lonitz, K., Barlakas, V., Eriksson, P., Mendrok, J., et al. (2021). Bulk hydrometeor optical properties for microwave and sub-millimetre radiative transfer in RTTOV-SCATT v13.0. *Geoscientific Model Development*, *14*(12), 7497–7526. https://doi.org/10.5194/gmd-14-7497-2021

Hersbach, H., Bell, B., Berrisford, P., Hirahara, S., Horányi, A., Muñoz-Sabater, J., et al. (2020). The ERA5 global reanalysis. *Quarterly Journal of the Royal Meteorological Society*, *146*(730), 1999–2049. https://doi.org/10.1002/qj.3803

Kilic, L., Prigent, C., Jimenez, C., Turner, E., Hocking, J., English, S., et al. (2023). Development of the SURface fast emissivity model for ocean (SURFEM-Ocean) based on the PARMIO radiative transfer model. *Earth and Space Science*, *10*(11), e2022EA002785. https://doi.org/10.1029/2022EA002785

Mattioli, V., Accadia, C., Prigent, C., Crewell, S., Geer, A., Eriksson, P., et al. (2019). Atmospheric gas absorption knowledge in the submillimeter: Modeling, field measurements, and uncertainty quantification. *Bulletin of the American Meteorological Society*, *100*(12), ES291–ES295. https://doi.org/10.1175/BAMS-D-19-0074.1

May, E., & Eriksson, P. (2025). The ice cloud imager: Retrieval of frozen water mass profiles. *Atmospheric Measurement Techniques*, *18*(23), 7243–7266. https://doi.org/10.5194/amt-18-7243-2025

May, E., Rydberg, B., Kaur, I., Mattioli, V., Hallborn, H., & Eriksson, P. (2024). The ice cloud imager: Retrieval of frozen water column properties. *Atmospheric Measurement Techniques*, *17*(19), 5957–5987. https://doi.org/10.5194/amt-17-5957-2024

Pfreundschuh, S., Fox, S., Eriksson, P., Duncan, D., Buehler, S. A., Brath, M., et al. (2022). Synergistic radar and sub-millimeter radiometer retrievals of ice hydrometeors in mid-latitude frontal cloud systems. *Atmospheric Measurement Techniques*, *15*(3), 677–699. https://doi.org/10.5194/amt-15-677-2022

Rodgers, C. D. (2000). Inverse methods for atmospheric sounding: Theory and practice. In *Series on atmospheric, Oceanic and planetary physics* (Vol. 2). World Scientific. https://doi.org/10.1142/3171

Turner, E., Fox, S., Mattioli, V., & Cimini, D. (2022). *Literature review on microwave and sub-millimetre spectroscopy for MetOp second generation (Tech. Rep.)*. EUMETSAT. Retrieved from https://nwp-saf.eumetsat.int/site/download/members_docs/cdop-3_reference_documents/NWPSAF_report_submm_litrev.pdf

Waliser, D. E., Li, J. L. F., Woods, C. P., Austin, R. T., Bacmeister, J., Chern, J., et al. (2009). Cloud ice: A climate model challenge with signs and expectations of progress. *Journal of Geophysical Research*, *114*, D00A21. https://doi.org/10.1029/2008JD010015

Wehr, T., Kubota, T., Tzeremes, G., Wallace, K., Nakatsuka, H., Ohno, Y., et al. (2023). The EarthCARE mission – Science and system overview. *Atmospheric Measurement Techniques*, *16*(15), 3581–3608. https://doi.org/10.5194/amt-16-3581-2023

Wu, D. L., Jiang, J. H., Read, W. G., Austin, R. T., Davis, C. P., Lambert, A., et al. (2008). Validation of the aura mls cloud ice water content measurements. *Journal of Geophysical Research*, *113*(D15), D15S10. https://doi.org/10.1029/2007JD008931